SCIENTIFIC REPORTS

OPEN

# Proof of concept of a frequency-preserving and time-invariant metamaterial-based nonlinear acoustic diode

Received: 21 February 2019
Accepted: 23 May 2019
Published online: 02 July 2019

A. S. Gliozzi[1], M. Miniaci[2], A. O. Krushynska[3], B. Morvan[4], M. Scalerandi[1], N. M. Pugno[5,7,8] & F. Bosia[6]

**Acoustic filters and metamaterials have become essential components for elastic wave control in applications ranging from ultrasonics to noise abatement. Other devices have been designed in this field, emulating their electromagnetic counterparts. One such case is an acoustic diode or rectifier, which enables one-way wave transmission by breaking the wave equation-related reciprocity. Its achievement, however, has proved to be rather problematic, and current realizations display a number of shortcomings in terms of simplicity and versatility. Here, we present the design, fabrication and characterization of a device able to work as an acoustic diode, a switch and a transistor-like apparatus, exploiting symmetry-breaking nonlinear effects like harmonic generation and wave mixing, and the filtering capabilities of metamaterials. This device presents several advantages compared with previous acoustic diode realizations, including versatility, time invariance, frequency preserving characteristics and switchability. We numerically evaluate its efficiency and demonstrate its feasibility in a preliminary experimental realization. This work may provide new opportunities for the practical realization of structural components with one-way wave propagation properties.**

In acoustics as well as in electromagnetism, the invariance of the wave equation under time inversion leads to the fundamental property of reciprocity, i.e. symmetrical wave propagation between two points in space, independently of which is the source and which is the receiver. This has been widely exploited in the so-called time-reversal technique, which enables to focus on a source or scatterer by time-reversing and retransmitting the signal recorded by an array of transducers[1]. However, reciprocity is not necessarily desirable in all cases, especially when the goal is to isolate a source from its echos. Removal of unwanted reflections could indeed find numerous applications, such as acoustic one-way mirrors to prevent an ultrasound source from being disturbed by reflected waves[2,3], unidirectional sonic barriers to block environmental noise in a predefined direction[4], control of acoustic energy transmission in medical applications using focused ultrasound[5], and energy harvesting[6]. To achieve this, researchers in the field of acoustics and ultrasonics have drawn inspiration from electromagnetism, in the quest for a simple and efficient realization of an Acoustic Diode (AD) or rectifier. However, as illustrated by Maznev *et al.*[7], linear elastic systems cannot be exploited to create ADs or isolators because they do not violate the reciprocity principle, so that the symmetry needs to be broken, for instance by periodically varying the elastic properties

[1]Department of Applied Science and Technology, Politecnico di Torino, Corso Duca degli Abruzzi 24, 10129, Torino, Italy. [2]Empa, Laboratory of Acoustics and Noise Control, Überlandstrasse 129, 8600, Dübendorf, Switzerland. [3]Computational Mechanical and Materials Engineering, Engineering and Technology institute Groningen, Faculty of Science and Engineering, University of Groningen, Groningen, 9747AG, The Netherlands. [4]University of Le Havre, Laboratoire Ondes et Milieux Complexes, UMR CNRS 6294, 75 Rue Bellot, 76600, Le Havre, France. [5]Laboratory of Bio-Inspired and Graphene Nanomechanics, Department of Civil, Environmental and Mechanical Engineering, Universit di Trento, via Mesiano, 77, I-38123, Trento, Italy. [6]Department of Physics and Nanostructured Interfaces and Surfaces Centre, University of Torino, Via Pietro Giuria 1, 10125, Torino, Italy. [7]School of Engineering and Materials Science, Queen Mary University of London, Mile End Road, London, E1 4NS, United Kingdom. [8]Ket-Lab, Edoardo Amaldi Foundation, via del Politecnico snc, I-00133, Roma, Italy. Correspondence and requests for materials should be addressed to A.S.G. (email: antonio.gliozzi@polito.it) or F.B. (email: federico.bosia@unito.it)

in space and time or by means of the introduction of nonlinearity coupled with some other mechanism (e.g. attenuation)[7].

With this in mind, a periodical variation of elastic properties in space and time has been exploited in theoretical and numerical studies of one-dimensional systems described by the discrete nonlinear Schrödinger equation with spatially varying coefficients embedded in a linear lattice[8], or in continuous elastic systems with periodically-modulated elastic properties in space and time[9], or in non-reciprocal active acoustic metamaterials[10]. In other works, the introduction of nonlinearity has been the adopted strategy, such as in the 1-D design of a "superlattice" structure coupled with a nonlinear elastic medium[2], later realized experimentally using a contrast agent microbubble suspension to generate the nonlinearity[3], converting energy from the fundamental frequency to higher harmonics[7]. Since then, several experimental realizations of ADs or rectifiers based on different mechanisms have been achieved. In one case, unidirectional transmission was obtained through mode conversion, using a sonic crystal, rather than elastic nonlinearity[11]. In another, a mechanical energy switch and transistor are implemented by exploiting nonlinear dynamical effects of a granular crystal chain[12]. To break the transmission symmetry, another study proposed to use a subwavelength acoustic resonant ring cavity filled with a circulating fluid, splitting the degenerate azimuthal resonant modes, in analogy with the Zeeman effect in electromagnetism[13]. In another realization, a thin brass plate with single-sided periodical gratings immersed in water was shown to provide unidirectional transmission in a broad frequency range[14]. Finally, a passive multi-port structure with asymmetric sound transmission between neighbouring ports was presented[15]. Comprehensive reviews of these and other approaches can be found in[7,16], in the latter with special reference to information processing in phononic computing, while the optimization of a rectifier efficiency in periodic mass–spring lattices is discussed in[17].

Many of these approaches are based on designing periodic structures, mainly phononic crystals and elastic metamaterials, which have attracted much attention for their wave manipulation capabilities, including negative refraction[18], frequency Band Gap (BG) formation[19–21], wave filtering or focusing[22–25], scattering-free propagation[26] and acoustic cloaking[27]. Recent studies have shown how structural instabilities induced in "static" mechanical metamaterials can be exploited to achieve highly nonlinear dynamic response that can be tailored to requirements[28,29] and how weakly nonlinear monoatomic lattice chains can provide active control on elastic waves in phononic crystals[30]. These or other approaches can be exploited to generate the type of nonlinearity required to violate spatial reciprocity in elastic wave propagation[31]. On the other hand, phononic crystals and metamaterials are ideal candidates to efficiently realise large BGs[32,33] or to concentrate energy into selected frequency ranges[25,34].

In this paper, we propose the realization of an AD, based on the use of linear phononic crystals and elastic metamaterials, embedded between elastic nonlinear regions. The novelty of the device is that it is simultaneously time–invariant (in the sense that its physical properties are not modified externally from the forward to the backward propagation direction[35]) and frequency preserving. Furthermore, besides its functionality as a diode, the device can be activated or deactivated at will for other applications, transforming it into a switch with the additional possibility to tune the amplitude of the output signal. These characteristics are in general not concurrently present in other AD designs that exploit nonlinearity to break the propagation symmetry and to transfer energy from the fundamental to the harmonics, with a frequency variation from input to output. The originality of our approach also resides in the exploitation of the combined effects of two different features of nonlinear elastic wave propagation, i.e. higher order harmonic generation and wave mixing, which allow to preserve the operating frequency occuring in two different zones separated by the periodic (filtering) structure. We recall that wave mixing occurs when two longitudinal waves propagating through a nonlinear elastic zone interact and generate another longitudinal wave with a frequency given by the difference (and sum) of the frequencies of the two original waves.

## Working Principle

The working principle of the AD proposed in this study is illustrated in Fig. 1 and can be described as follows:

(i). *Propagation from left to right (LtR*, Fig. 1a): an input signal is injected (from $S_1$) into the device where it encounters a passband filter FB1 that selects a range of frequencies around $f_1$. These waves then travel through a first nonlinear elastic zone, named NL1, where a second frequency $f_2 = \frac{3}{2}f_1$ can be injected from the source $S_2$. In this case, the presence of nonlinearity generates higher harmonics and the sum and difference frequencies (wave mixing), including $f_2 - f_1 = f_0 = \frac{f_1}{2}$, which is a subharmonic of $f_1$. The next portion of the device, FB2, is a low-pass filter, which eliminates frequencies above $f_0$, and a second nonlinear zone, NL2, where the second harmonic $f_1 = 2f_0$ is generated. Finally, another passband filter (FB3) filters out $f_0$ and the harmonics higher than $f_1$, giving an overall output signal $f_1$ at the same frequency of the input.

(ii). *Propagation from right to left (RtL*, Fig. 1b*):* in this case, the input signal at $f_1$ travels through FB3 and through NL2 where higher harmonics are generated (but not $f_0$), and where no wave mixing process takes place (this breaks spatial reciprocity). The next portion of the device, FB2, filters out the full signal, so that no signal propagates through NL1 and FB1, generating no output from the device.

Notice that the source $S_2$ is present both in the forward and in the backward propagation (in this sense the AD is time invariant in its physical characteristics) and its role is to break spatial symmetry in the device. This mechanism allows us to overcome some of the difficulties in the practical realization encountered in other theoretical works that propose frequency-preserving ADs[36–38]. The present model/configuration has been conceived

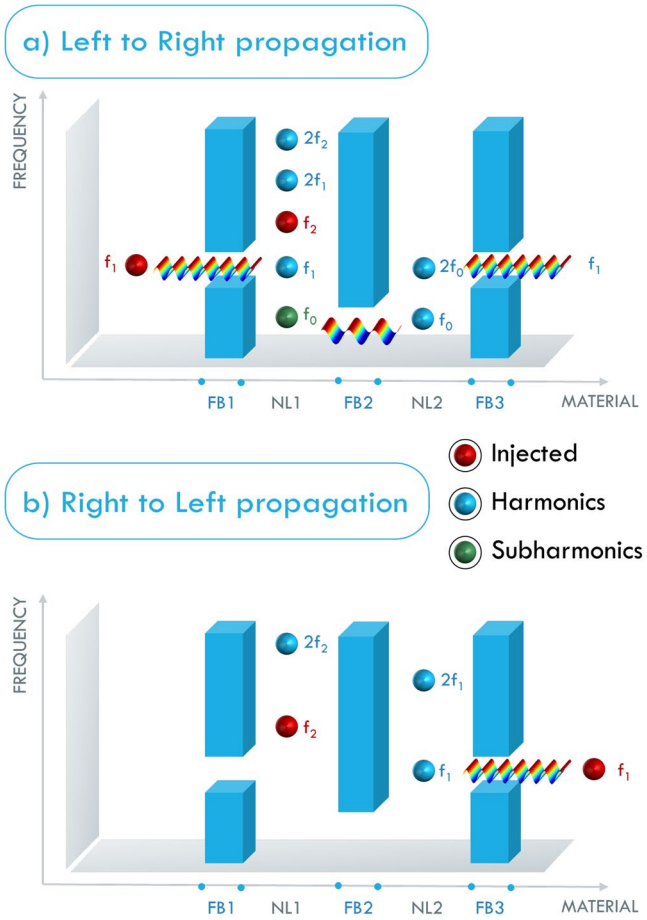


**Figure 1.** Schematic representation of the basic concept of the proposed AD for (**a**) left to right and (**b**) right to left propagation, respectively. $f_1$ and $f_2 = \frac{3}{2}f_1$ are the injected wave components, while $f_0 = \frac{1}{2}f_1$ is generated by wave mixing. The blue barriers represent the frequency BGs, between them are the nonlinear cavities (NL1 and NL2) where harmonic generation and wave mixing take place. The overall effect of the device is to trasmit $f_1$ from left to right, but not from right to left.

for monochromatic inputs, as usually done for nonlinearity-based ADs. More complicated designs can be considered by imposing a non-monochromatic wave injected by the source $S_2$. However, this is beyond the scope of this work.

## Results

In this work, we exploited the filtering properties of two different types of phononic crystals, described in the Methods Section and Supplemental Material, for the Filtering Barrier regions of the device. To verify the feasibility and functionality of the device, we first performed wide-ranging simulations of its general characteristics (Figs 2 and 3) and then verified results in a preliminary experimental realization (Fig. 4).

**Numerical simulations.** Figure 2a shows a schematic of the sample considered in the simulations described in the Methods section. The excitation signal (a sinusoidal wave) is uniformly applied at the left boundary of FB1 (for LtR propagation) or at the right boundary of FB3 (for RtL propagation). We assume reflecting conditions at the boundaries that are free from excitation.

With this configuration, we perform wave propagation simulations to demonstrate the feasibility of the AD. For the LtR (RtL) propagation, we inject a monochromatic wave of frequency $f_1 = 600$ kHz on the left (right) side of the device and the corresponding $f_2 = 900$ kHz in the left cavity. The output signal is recorded on the left (right) side of the sample (T1 in Fig. 2a). Figure 2 shows the Fast Fourier Transform (FFT) of the signals for LtR (b–d) and RtL (e–g), respectively. The signals are recorded at the input of the device (b,e), in the first cavity on the left (c,f) and at the output (d,g). While $f_1$ propagates from LtR, no signal is detected at the receiver when the propagation is in the other direction. In the output of the RtL propagation, only noise is present and no energy transmission is detectable. This proves the very good performance of the acoustic diode device. The difference between the two cases (reported in the upper and lower parts of Fig. 2(b–g), respectively) lies in the generation in the left cavity of the frequency $f_0$, which is the only component that can propagate from NL1 to NL2. In the left cavity (Fig. 2c) we observe the presence of the harmonics of the foundamental frequency generated by the

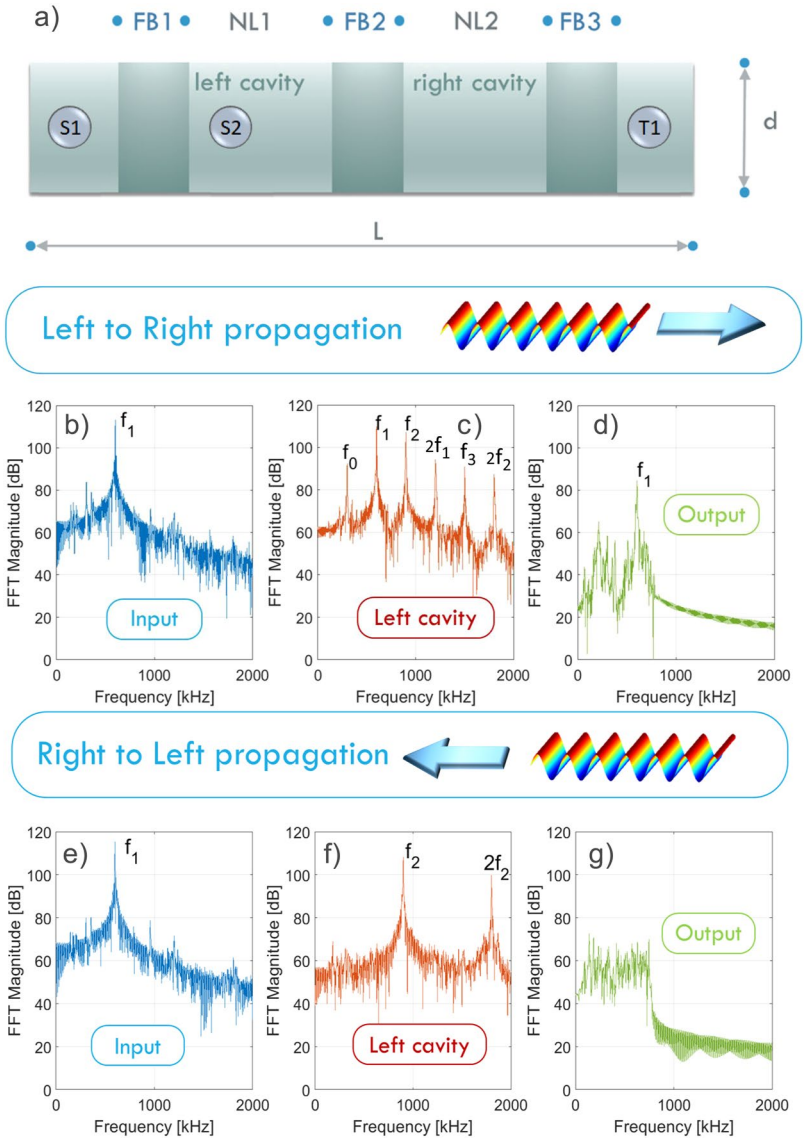


**Figure 2.** Numerical simulations. Schematic of the considered sample (**a**); Fast Fourier Transforms of the signal recorded in the input (**b**,**e**), in the first cavity on the left (**c**,**f**) and at the output (**d**,**g**), for the two propagation directions (LtR and RtL in the first and second rows, respectively).

two sources and the two other frequencies $f_0 = f_2 - f_1$ and $f_3 = f_1 + f_2$, due to the nonlinear frequency mixing process.

Although any mechanism able to generate sub-harmonics[39,40] of $f_1$ can be appropriate, the mechanism based on wave mixing adopted here to generate $f_0$ has several advantages. The first is that wave mixing is an extremely efficient way to produce sub-harmonics and no threshold mechanism appears to be present. Moreover, the source $S_2$ can be tuned in order to decrease or increase the amplitude of the $f_0$ component, and in the limit case to suppress it. Thus, the device can be used as an *on-off* or an *amplitude-tuning* switch. Two different simulations are presented to demonstrate these applications.

In the first case, the source $S_2$ (the pump) is switched on/off at regular time intervals and the corresponding output recorded (Fig. 3a). It is clear that the signal is prevented from propagating when the source $S_2$ is switched off. This is also evident in the FFT analysis performed by windowing the time signal for the two different cases ($S_2$ on/off in Fig. 3b). This demonstrates the use of the AD as an on/off switch.

The same numerical experiment is then repeated at increasing amplitude of the pump ($S_2$) while keeping the amplitude of $S_1$ fixed. Since the amplitude of the $f_0$ component (the subharmonic of the input) is proportional to the product of the two mixed frequency amplitudes, it is possible to vary the output signal amplitude by tuning the amplitude of the pump ($S_2$, in this case), as shown in Fig. 3(c–i). This generates the possibility to realize a switch with a variable amplitude output (i.e. a transistor-like apparatus). Moreover, from a theoretical point of view, this provides the possibility of considerably increasing the efficiency of the device by pumping energy from $S_2$ and increasing the output amplitude at will. Indeed, despite the presence of an additional nonlinear process,

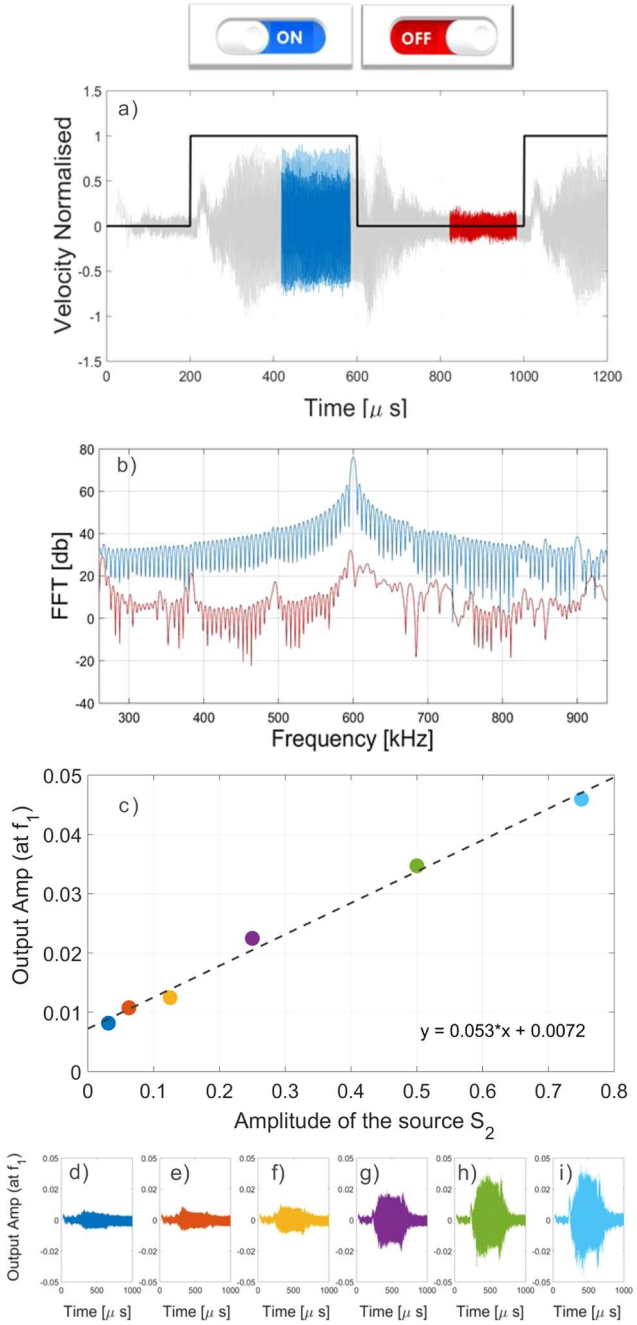


**Figure 3.** Acoustic on-off and amplitude-tunable switch. By switching on/off the source $S_2$, the wave generated by $S_1$ can/cannot propagate through the device. This is visible in numerical simulations in both the (**a**) time and (**b**) frequency domain. The FFT performed over different time windows (highlighted with different colors in subplot (**a**)) shows the different frequency content of the propagating wave. Results relative to a tuning-amplitude switch are shown in (**c**): the output amplitude linearly increases as a function of the pump amplitude $S_2$, for constant input amplitude, $S_1$ (the equation of the fitting function is also reported); (**d**–**i**) Corresponding outputs signals.

theoretical considerations and numerical simulations indicate that the efficiency of the AD proposed could be greatly increased by playing with the nonlinear parameters and by tuning the amplitude of the pumping energy, as discussed in the Supplemental Material. From a practical point of view, a large amplification at the pump transducer ($S_2$) may be limited by spurious nonlinear effects and by the large amount of energy required. Nevertheless, considering reasonable experimental limitations, we could still achieve an efficiency of the order of a few percent, which is comparable to the results obtained with other nonlinear-based ADs involving a single nonlinear process[3,41]. Furthermore, more efficient systems to generate nonlinearity could also be employed to further improve

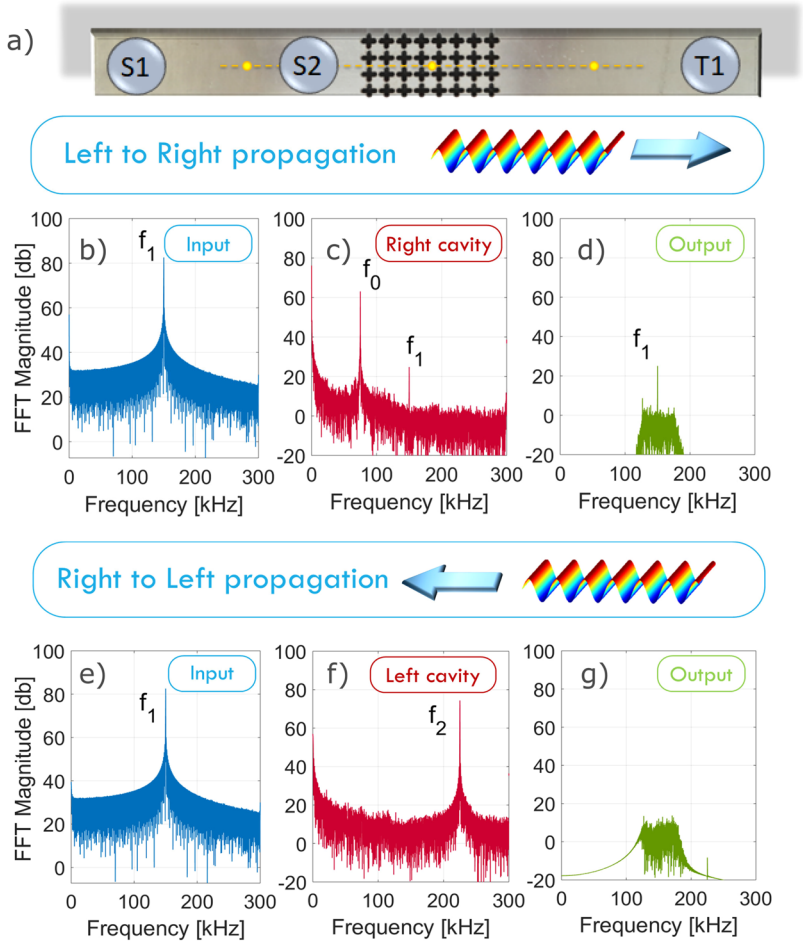


**Figure 4.** Experimental set up (**a**) and results for LtR (**b**–**d**) and RtL (**e**–**g**) propagation. In the first and second columns, the FFT of the injected signal (**b**,**e**) and of the output (**c**,**f**) in the right and left cavities, are reported, respectively. The third column shows the simulated effect on the FFT of the output of the phononic barriers in the full device.

the efficiency of the device, e.g. that presented in ref.[42], so that the performance can be enhanced by two orders of magnitude.

**Experimental realization.** The discussed design of the AD is quite general and can be realized with different nonlinearity types, filtering characteristics or optimized properties. We demonstrate its feasibility through the experimental realization of a prototype, shown in Fig. 4a, representing the central part of the device, which is responsible for the breaking of reciprocity. The experimental procedure is discussed in detail in the Methods section. Two source trandsucers ($S_1$ and $S_2$) are placed in the first nonlinear cavity (NL1), and a target transducer ($T_2$) in the second nonlinear cavity NL2. In this case, to exploit the phononic barrier characteristics, we set $f_1 = 150$ kHz and $f_2 = 225$ kHz.

Figure 4(b–d) illustrate LtR propagation, as detected by the laser vibrometer, while Fig. 4(e–g) refer to RtL propagation. For the LtR propagation, $S_1$ is placed in NL1 and $T_1$ in NL2, while for LtR, they are inverted, leaving the position of $S_2$ unchanged. The FFT of the input signal injected at the source $S_1$ and of the output are shown in the first and in the second columns, respectively. The filtering action of FB1 and FB3 in the complete device, i.e. the effect of the phononic barriers, is simulated here in post-processing by imposing a numerical band-pass filter (centered around $f_1 = 150$ kHz) on the output signals (Fig. 4d,g). Despite the relatively small amplitudes, the symmetry breaking in the wave propagation for the frequency $f_1$ is evident in the two considered propagation directions. The difference in the output obtained in the left and right propagation demonstrates the functionality of the AD.

## Conclusions

In summary, we have presented numerical and experimental results demonstrating the feasibility of an acoustic diode based on alternating nonlinear elastic and metamaterial frequency-filtering regions, with time-invariant, frequency preserving characteristics. The design concept is on the one hand rather simple, since it is based on the sequential repetition of only two basic building blocks, i.e. nonlinear cavities and metamaterial-based frequency

filters (low-pass and bandpass); on the other hand, it is sufficiently general to allow flexibility in its realization, involving different combinations of nonlinearity and BG mechanisms, and the use of phononic crystals or resonant metamaterials provides the opportunity to tune and scale results to the desired device sizes and frequency ranges. Additionally, the adoption of an input monochromatic driving signal allows the adaptation of the concept to different types of devices, such as switches or transistors, which can be exploited in practical applications in the field of acoustics or ultrasonics[43]. These can potentially be coupled and integrated with recently introduced metamaterial-based sensors for damage detection and localization[25] or for other advanced signal manipulation purposes, including in quantum acoustodynamics[44]. On the other hand, AD-based devices could also be exploited for energy harvesting, exploiting their unidirectional transmission characteristics for elastic wave energy trapping. Improvements in the nonlinear elasticity generation mechanisms are currently under study to provide improved device stability and efficiency, potentially leading to its integration in advanced apparatuses requiring one-way transmission.

## Methods

**Numerical calculations.** In numerical simulations, we model the device as an Aluminum plate with mass density $\rho_1 = 2700\,\mathrm{kg/m^3}$, Young modulus $E = 70\,\mathrm{GPa}$, and Poisson ratio $\nu = 0.33$ and in-plane dimensions $L = 105\,\mathrm{mm}$ and $d = 6.6\,\mathrm{mm}$ (Fig. 2a). The core of the device, in which reciprocity is broken, is composed by two nonlinear zones (NL1 and NL2 in Fig. 2a), separated by a metamaterial (FB2).

The nonlinear sections NL1 and NL2 are realized by considering a zone of diffuse nonlinearity, and the numerical nonlinear parameters are set in order to produce about 10% of harmonics and subharmonics. These two nonlinear zones are placed between two filters made of metamaterials or phononic crystals, which confine the frequency components of the wavefield falling in their BGs, creating a sort of resonant cavity (also denominated left and right cavities in the following). The dimensions of these regions and of the nonlinear elements can be tailored to enhance the desired frequencies through resonance effects ($f_0$ in the left, and $f_1$ in the right cavity). A nonclassical nonlinear model[45–47], implemented using a Preisach-Mayergoyz[48] space representation, is adopted to simulate the nonlinear elastic response of these zones.

The structure of each metamaterial/phononic crystal part (FB1-FB3) is described in detail in the Supplementary Material together with its dispersion characteristics. The scalability of the results is guaranteed by the fact that the geometry of the constituent elements can easily be tuned to shift the pass bands to the desired frequencies.

**Experimental.** For the experimental verification of the proposed working principle, we use a $380 \times 40 \times 6\,\mathrm{mm^3}$ aluminium plate ($\rho = 2700\,\mathrm{kg/m^3}$, $E = 70\,\mathrm{GPa}$ and $\nu = 0.33$) with a phononic crystal region representing the filtering barrier (FB2 in Fig. 1). The phononic crystal is located between two regions that represent the left (with NL1) and right (with NL2) cavities in Fig. 1. FB2 consists of a 2D array of $4 \times 8$ cross-like cavities, fabricated using waterjet cutting, with a lattice parameter of $a = 10\,\mathrm{mm}$ (see Supplemental Material for geometrical details). Dimensions have been designed so as to suppress frequencies from 124 kHz to 175 kHz and 191 kHz to 236 kHz, in the propagation from one cavity to the other (see Supplemental Material for further details). It follows that the working frequency of this AD is $f_1 = 150\,\mathrm{kHz}$, while the pump $S_2$ needs to be set at a frequency $f_2 = 225\,\mathrm{kHz}$. In this simplified realization, in the LtR propagation, the two sources ($S_1$ and $S_2$) are located in the same cavity on the left, while the receiver ($T_1$) is situated in the right cavity, as shown in Fig. 4a. The nonlinearity is generated in the two cavities, by superposing onto the plate a small object coupled with a drop of water[25]. The clapping of the surfaces, due to the action of the elastic wavefield propagating in the plate gives rise to typical nonlinear effects (i.e. harmonics and wave mixing). However, this method to generate nonlinearity is not sufficiently stable to allow tunability of the output amplitude through the $S_2$ input amplitude, so that the transistor-like switch functionality cannot be implemented. However, it serves the purpose of demonstrating the diode functionality in a proof-of-concept experiment.

In the experiments, the emitting piezoelectric contact transducer was connected to an arbitrary waveform generator (Agilent 33500B) through a 50 dB linear amplifier (FLC Electronics A400). The receiving transducer/laser interferometer was connected to an oscilloscope (Agilent Infiniium DSO9024H) for data acquisition.

## References


1. Fink, M. *et al*. Time-reversed acoustics. *Rep. Progr. Phys.* **63**, 1933–1995 (2000).
2. Liang, B., Yuan, B. & Cheng, J.-C. Acoustic Diode: Rectification of Acoustic Energy Flux in One-Dimensional Systems. *Phys. Rev. Lett.* **103**, 104301 (2009).
3. Liang, B., Zou, X.-Y., Zhang, D. & Cheng, J.-C. An acoustic rectifier. *Nat. Mater.* **9**, 989–992 (2010).
4. Li, B. Now you hear me, now you don't. *Nat. Mater.* **9**, 962–963 (2010).
5. Haar, G. T. & Coussios, C. High intensity focused ultrasound: Physical principles and devices. *Int. J. Hyperther.* **23**(2), 89–104 (2007).
6. Liu, K. & He, S. Truly trapped rainbow by utilizing nonreciprocal waveguides. *Sci. Rep.* **6**, 30206 (2016).
7. Maznev, A., Every, A. & Wright, O. Reciprocity in reflection and transmission: What is a 'phonon diode'? *Wave Motion* **50**, 776–784 (2013).
8. Lepri, S. & Casati, G. Asymmetric Wave Propagation in Nonlinear Systems. *Phys. Rev. Lett.* **106**, 164101 (2011).
9. Trainiti, G. & Ruzzene, M. Non-reciprocal elastic wave propagation in spatiotemporal periodic structures. *New J. Phys.* **18**, 083047 (2016).
10. Popa, B. I. & Cummer, S. A. Non-reciprocal and highly nonlinear active acoustic metamaterials. *Nat. Commun.* **5**, 3398 (2014).
11. Li, X.-F. *et al*. Tunable Unidirectional Sound Propagation through a Sonic-Crystal-Based Acoustic Diode. *Phys. Rev. Lett.* **106**, 084301 (2011).
12. Li, F., Anzel, P., Yang, J., Kevrekidis, P. G. & Daraio, C. Granular acoustic switches and logic elements. *Nat. Commun.* **5**, 5311 (2014).

13. Fleury, R., Sounas, D. L., Sieck, C. F., Haberman, M. R. & Alù, A. Sound isolation and giant linear nonreciprocity in a compact acoustic circulator. *Science* **343**, 516–519 (2014).
14. Sun, H.-X., Zhang, S.-Y. & Shui, X.-J. A tunable acoustic diode made by a metal plate with periodical structure. *Appl. Phys. Lett.* **100**, 103507 (2012).
15. Zhu, Y.-F. *et al*. Asymmetric sound transmission in a passive non-blocking structure with multiple ports. *Appl. Phys. Lett.* **109**, 103504 (2016).
16. Sklan, S. R. Splash, pop, sizzle: Information processing with phononic computing. *AIP Advances* **5**, 053302 (2015).
17. Ma, C., Parker, R. G. & Yellen, B. B. Optimization of an acoustic rectifier for uni-directional wave propagation in periodic mass–spring lattices. *J. Sound Vib.* **332**, 4876–4894 (2013).
18. Morvan, B., Tinel, A., Hladky-Hennion, A.-C., Vasseur, J. & Dubus, B. Experimental demonstration of the negative refraction of a transverse elastic wave in a two-dimensional solid phononic crystal. *Appl. Phys. Lett.* **96**, 101905 (2010).
19. Kushwaha, M. S., Halevi, P., Dobrzynski, L. & Djafari-Rouhani, B. Acoustic band structure of periodic elastic composites. *Phys. Rev. Lett.* **71**, 2022 (1993).
20. Martinez-Sala, R. *et al*. Sound attenuation by sculpture. *Nature* **378**, 241 (1995).
21. Fraternali, F. & Amendola, A. Mechanical modeling of innovative metamaterials alternating pentamode lattices and confinement plates. *J. Mech. Phys. Solids* **99**, 259–271 (2017).
22. Yang, S. *et al*. Focusing of Sound in a 3D Phononic Crystal. *Phys. Rev. Lett.* **93**, 024301 (2004).
23. Brun, M., Guenneau, S., Movchan, A. B. & Bigoni, D. Dynamics of structural interfaces: filtering and focussing effects for elastic waves. *J. Mech. Phys. Solids* **58**, 1212 (2010).
24. Gliozzi, A. S., Miniaci, M., Bosia, F., Pugno, N. M. & Scalerandi, M. Metamaterials-based sensor to detect and locate nonlinear elastic sources. *Appl. Phys. Lett.* **107**, 161902 (2015).
25. Miniaci, M. *et al*. Proof of Concept for an Ultrasensitive Technique to Detect and Localize Sources of Elastic Nonlinearity Using Phononic Crystals. *Phys. Rev. Lett.* **118**, 214301 (2017).
26. Miniaci, M., Pal, R. K., Morvan, B. & Ruzzene, M. Experimental Observation of Topologically Protected Helical Edge Modes in Patterned Elastic Plates. *Phys. Rev. X* **8**, 031074 (2018).
27. Zhang, S., Xia, C. & Fang, N. Broadband Acoustic Cloak for Ultrasound Waves. *Phys. Rev. Lett.* **106**, 024301 (2011).
28. Nadkarni, N., Daraio, C. & Kochmann, D. M. Dynamics of periodic mechanical structures containing bistable elastic elements: From elastic to solitary wave propagation. *Phys. Rev. E* **90**, 023204 (2014).
29. Bertoldi, K. Harnessing Instabilities to Design Tunable Architected Cellular Materials. *Annu. Rev. Mater. Res.* **47**, 51–61 (2017).
30. Wang, Y.-Z., Li, F.-M. & Wang, Y.-S. Influences of active control on elastic wave propagation in a weakly nonlinear phononic crystal with a monoatomic lattice chain. *Int. J. Mech. Sci.* **106**, 357–362 (2016).
31. Scalerandi, M., Gliozzi, A. S. & Bruno, C. L. E. Detection and location of cracks using loss of reciprocity in ultrasonic waves propagation. *J. Acoust. Soc. Am.* **131**, EL81 (2012).
32. Deymier, P. & Dobrzynski, L. Discrete one-dimensional phononic and resonant crystals in *Acoustic Metamaterials and Phononic Crystals* (Ed. Deymier, P.A.), **13** (Springer, 2013).
33. Krushynska, A. O., Miniaci, M., Bosia, F. & Pugno, N. Coupling local resonance with Bragg band gaps in single-phase mechanical metamaterials. *Extreme Mech. Lett.* **12**, 30–36 (2017).
34. Carrara, M. *et al*. Metamaterial-inspired structures and concepts for elastoacoustic wave energy harvesting. *Smart Mater. Struct.* **22**, 065004 (2013).
35. Tsakmakidis, K. L. *et al*. Breaking Lorentz reciprocity to overcome the time-bandwidth limit in physics and engineering. *Science* **356**, 1260 (2017).
36. Liu, C., Du, Z., Sun, Z., Gao, H. & Guo, X. Frequency-Preserved Acoustic Diode Model with High Forward-Power-Transmission Rate. *Phys. Rev. Appl.* **3**, 064014 (2015).
37. Gu, Z.-M., Hu, J., Liang, B., Zou, X.-Y. & Cheng, J.-C. Broadband non-reciprocal transmission of sound with invariant frequency. *Sci. Rep.* **6**, 19824 (2016).
38. Chen, H., Norris, A. N., Haberman, M. R. & Huang, G. L. Non-reciprocal wave propagation in modulated elastic metamaterials. *Proc. R. Soc. A* **473**, 20170188 (2017).
39. Alippi, A. *et al*. Low threshold subharmonic generation in composite structures with Cantor-like code. *Phys. Rev. Lett.* **69**, 3318 (1992).
40. Bosia, F., Pugno, N. & Carpinteri, A. Subharmonic generation in physical systems: An interaction-box approach. *Wave Motion* **43**, 689–699 (2006).
41. Boechler, N., Theocharis, G. & Daraio, C. Bifurcation-based acoustic switching and rectification. *Nat. Mater.* **10**, 665 (2011).
42. Fu, C., Wang, B., Zhao, T. & Chen, C. Q. High efficiency and broadband acoustic diodes. *Appl. Phys. Lett.* **112**, 051902 (2018).
43. Bilal, O. R., Foehr, A. & Daraio, C. Bistable metamaterial for switching and cascading elastic vibrations. *PNAS* **114**, 4603–4606 (2017).
44. Manenti, R. *et al*. Circuit quantum acoustodynamics with surface acoustic waves. *Nat. Comm.* **8**, 975 (2017).
45. Ulrich, T. J., Johnson, P. A. & Guyer, R. A. Interaction Dynamics of Elastic Waves with a Complex Nonlinear Scatterer through the Use of a Time Reversal Mirror. *Phys. Rev. Lett.* **98**, 104301 (2007).
46. Gliozzi, A. S. & Scalerandi, M. Modeling dynamic acousto-elastic testing experiments: Validation and perspectives. *J. Acoust. Soc. Am.* **136**(4), 1530 (2014).
47. Delsanto, P. P. & Scalerandi, M. Modeling nonclassical nonlinearity, conditioning, and slow dynamics effects in mesoscopic elastic materials. *Phys. Rev. B* **68**, 064107 (2003).
48. Mayergoyz, I. D. Hysteresis models from the mathematical and control theory points of view. *J. Appl. Phys.* **57**, 3803 (1985).


## Acknowledgements

M.M. has received funding from the European Union's Horizon 2020 research and innovation program under the Marie Sk lodowska-Curie Grant Agreement No. 754364. N.M.P. is supported by the European Commission under the Graphene Flagship Core 2 Grant No. 785219 (WP14 "Composites") and FET Proactive "Neurofibres" Grant No. 732344 as well as by the Italian Ministry of Education, University and Research (MIUR) under the "Departments of Excellence" grant L. 232/2016, the ARS01-01384-PROSCAN Grant and the PRIN-20177TTP3S. F.B. is supported by H2020 FET Proactive Neurofibres Grant No. 732344, by project Metapp (n. CSTO160004) co-funded by Fondazione San Paolo, and by the Italian Ministry of Education, University and Research (MIUR) under the "Departments of Excellence" grant L. 232/2016.

## Author Contributions

A.S.G. conceived the idea and drafted the manuscript, A.S.G. and M.M. performed simulations and experiments, B.M. performed experiments, A.K. performed simulations, M.S., F.B. and N.M.P. contributed to the idea and data interpretation, all the authors contributed to the finalization of the manuscript.

## Additional Information

**Supplementary information** accompanies this paper at https://doi.org/10.1038/s41598-019-44843-7.

**Competing Interests:** The authors declare no competing interests.

**Publisher's note:** Springer Nature remains neutral with regard to jurisdictional claims in published maps and institutional affiliations.

# Supplemental Material for "A frequency-preserving and time-invariant metamaterial-based nonlinear acoustic diode"

A. S. Gliozzi,[1,*] M. Miniaci,[2,†] A. O. Krushynska,[3] B. Morvan,[4] M. Scalerandi,[1] N. M. Pugno,[5,‡] and F. Bosia[6]

[1]*Department of Applied Science and Technology, Politecnico di Torino, Corso Duca degli Abruzzi 24, 10129 Torino, Italy*

[2]*Enpa, Laboratory of Acoustics and Noise Control, Überlandstrasse 129, 8600 Dübendorf, Switzerland*

[3]*Engineering and Technology Institute Groningen, Faculty of Science and Engineering, University of Groningen, Groningen 9747AG, the Netherlands*

[4]*University of Le Havre, Laboratoire Ondes et Milieux Complexes, UMR CNRS 6294, 75 Rue Bellot, 76600 Le Havre, France*

[5]*Laboratory of Bio-Inspired and Graphene Nanomechanics, Department of Civil, Environmental and Mechanical Engineering, Università di Trento, via Mesiano, 77, I-38123 Trento, Italy*

[6]*Department of Physics and Nanostructured Interfaces and Surfaces Centre, University of Torino, Via Pietro Giuria 1, 10125 Torino, Italy*

(Dated: May 8, 2019)

*Electronic address: antonio.gliozzi@polito.it

†Also at: University of Le Havre, Laboratoire Ondes et Milieux Complexes, UMR CNRS 6294, 75 Rue Bellot, 76600 Le Havre, France

‡Also at: School of Engineering and Materials Science, Queen Mary University of London, Mile End Road, London E1 4NS, United Kingdom and Ket-Lab, Edoardo Amaldi Foundation, via del Politecnico snc, I-00133 Roma, Italy

## I. NUMERICAL MODELS

We first provide a detailed geometrical description of the filtering barriers FBi (with $i \in [1, 2, 3]$) presented in Fig. 1 of the main text, along with their dynamical behaviour in terms of band gaps (BGs) and pass bands.

### A. Design of the filtering barrier 1 (FB1) and filtering barrier 3 (FB3)

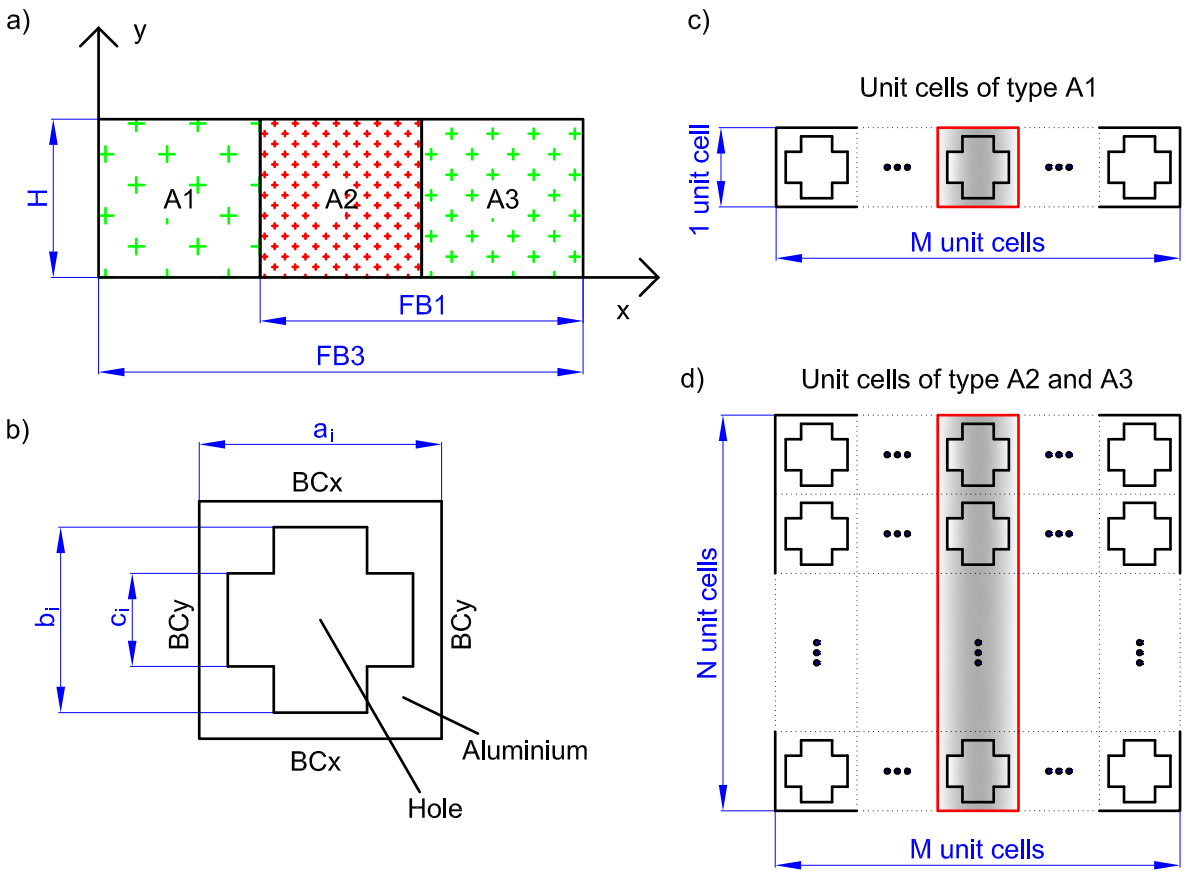


FIG. SM1: (a) Schematic representation of the FB1 and FB3 regions made of (b) periodic cross-like holes in an aluminium matrix and (c,d) their geometrical arrangements in $x$ and $y$ directions within the $A1$, $A2$ and $A3$ regions. The geometrical parameters $a_i$, $b_i$, $c_i$ of the unit cells are reported in Table I and the mechanical properties given in the text.

Fig. SM1a shows a schematic representation of the filtering barrier 1 (FB1) and filtering barrier 3 (FB3) regions.

TABLE I: Geometrical parameters for the unit cells presented in regions $A1$, $A2$ and $A3$ shown in Fig. SM1.

| Geometrical parameter | Value [mm] | | |
|---|---|---|---|
| | case $i = 1$ | case $i = 2$ | case $i = 3$ |
| $a_i$ | 6.60 | 0.66 | 1.20 |
| $b_i$ | $0.78{\cdot}a_1$ | $0.90{\cdot}a_2$ | $0.95{\cdot}a_3$ |
| $c_i$ | $0.18{\cdot}a_1$ | $0.20{\cdot}a_2$ | $0.20{\cdot}a_3$ |

FB1 is made of two phononic regions, namely $A2$ and $A3$ whereas FB3 is made of three phononic regions, namely $A1$, $A2$ and $A3$. All these regions are characterized by the presence of periodic cross-like holes into an aluminium matrix (Fig. SM1b) with the following mechanical properties: $\rho = 2700$ kg/m$^3$, $E = 70$ GPa and $\nu = 0.33$. The geometrical parameters $a_i$, $b_i$ and $c_i$ of the unit cells are reported in Table I and are chosen so as to provide proper filtering characteristics in specific frequency ranges (see Fig. 1 of the main text and Fig. SM3 of the next section). The number of unit cells chosen along the $y$-direction ($N$ in Figs. SM1c,d) derives from the choice of adopting the same height $H = 6.6$ mm for the entire device, whereas the number of repeated unit cells along the $x$-direction ($M$ in Figs. SM1c,d)) is dictated by the need to achieve an attenuation of the wave amplitude within the BG frequencies of at least one order of magnitude [1].

### B. Design of the filtering barrier 2 (FB2)

Fig. SM2 shows a schematic representation of the filtering barrier 2 (FB2). FB2 is made of locally resonant structures using heavy coated inclusions (highlighted in red in the figure) connected by thin ligaments. This choice is principally due to the type of filtering action required by FB2, i.e. a low pass band filter. The dispersion diagram originated by a single locally resonant structure adapts well to this need (see Fig. SM4 in the next section), contrary to the cases of FB1 and FB2, where pass bands within a lower frequency and a higher frequency filtering regions are required. Furthermore, this choice allows to minimize the size of the device, compared to using phononic crystals for the FB2 region, too. The resonators and ligament dimensions are reported in Table II and are tailored to provide

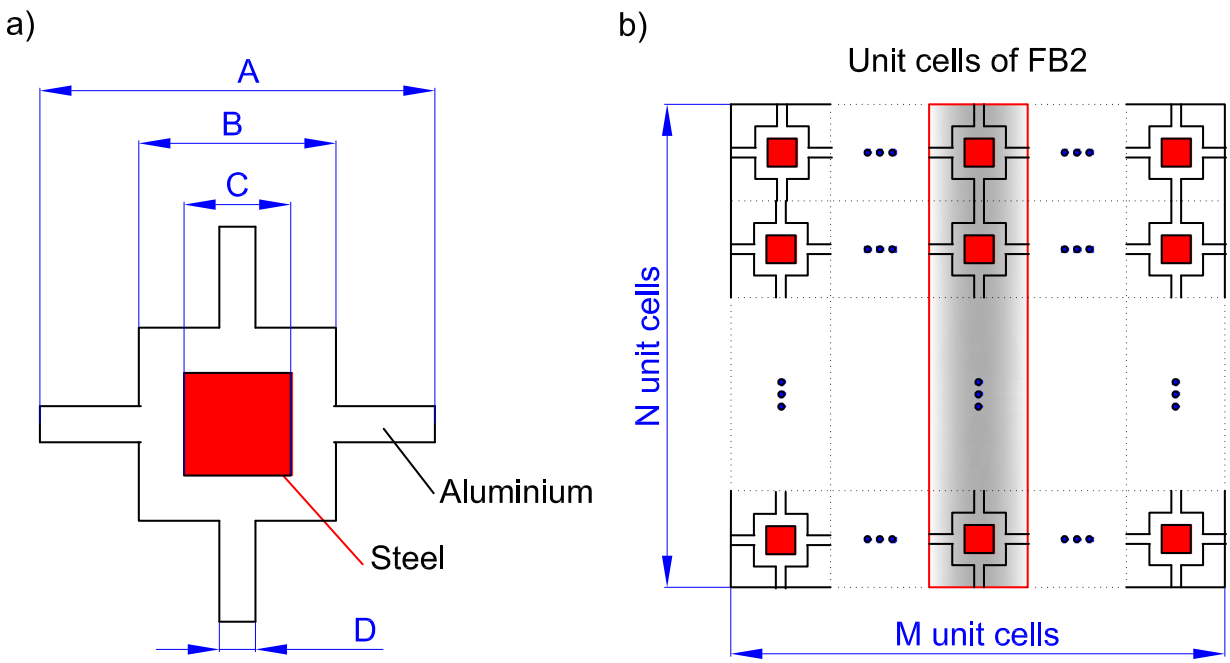


FIG. SM2: Schematic representation of the FB2 region made of (a) a locally resonant structures using heavy coated inclusions connected by thin ligaments. The resonators are square in shape and their dimensions are tailored to define the required properties of the barrier. The geometrical parameters of the unit cell are reported in Table II ($\rho = 2700$ kg/m$^3$, $E = 70$ GPa and $\nu = 0.33$) while the internal core made of steel has the following properties: $\rho = 7784\,\mathrm{kg/m^3}$, $E = 207\,\mathrm{GPa}$ and $\nu = 0.30$.

proper filtering abilities in specific frequency ranges (see Fig. 1 of the main text and Fig. SM4 of the next section). The geometrical parameters of the unit cell are reported in Table II. The matrix is made of aluminium ($\rho = 2700$ kg/m$^3$, $E = 70$ GPa and $\nu = 0.33$) while the internal core made of steel with the following properties: $\rho = 7784$ kg/m$^3$, $E = 207$ GPa and $\nu = 0.30$.

As in the previous case, the number of unit cells chosen along the $y$-direction ($N$ in Figs. SM2b) derives from the choice of adopting the same height $H = 6.6$ mm for the entire the device, whereas the number of repeated unit cells along the $x$-direction ($M$ in Figs. SM2b)) is dictated by the need to achieve an attenuation of the wave amplitude within the BG frequencies of at least one order of magnitude [1].

TABLE II: Geometrical parameters for the unit cell presented in Fig. SM2a.

| Geometrical parameter | Value [mm] |
|---|---|
| A | 1.65 |
| B | 1.15 |
| C | 0.82 |
| D | 0.07 |

## II. NUMERICAL RESULTS

In this section, dispersion diagrams for the regions described in the previous section are computed by applying the Bloch-Floquet theory. This allowed to consider only one so-called unit cell, i.e. the smallest representative geometry for computing the dispersion diagram [2]. The numerical models are implemented in a 2D-plane strain assumption. Cells are meshed by means of 4-node quadrilateral elements of maximum size $L_{FE} = 0.1$ mm in order to provide accurate eigensolutions up to the maximum frequency of interest of 2500 kHz. The band structures are derived assuming periodic (in the $x$-direction) and free (in the $y$-direction) boundary conditions at the edges of the cell domains due to the finite dimensions of the considered structures. The resulting eigenvalue problem $(\mathbf{K} - \omega^2\mathbf{M})\mathbf{u} = \mathbf{0}$ is solved by varying the wave vector $k_x$ values along the first irreducible Brillouin zone boundary $\Gamma - X$ (since the periodicity is only in the $x$-direction).

### A. Dispersion diagrams of the A1, A2 and A3 regions

Figure SM3 presents the band diagram for the unit cells composing regions A1, A2 and A3 in terms of reduced wavevector $k^* = k_x \cdot ai/\pi$ with $ai$ given in Table I. It is possible to see how the region A1 (Fig. SM3a) provides filtering lower frequencies ($f < f_1$) whereas regions A2 and A3 (Fig. SM3b,c) filter $f > f_1$ (BGs are highlighted by light pink rectangles).

### B. Dispersion diagrams of the FB2

Figure SM4 presents the band diagram for FB2 in terms of reduced wavevector $k^* = k_x \cdot A/\pi$ with $A$ given in Table II. It is possible to see how FB2 provides filtering for all

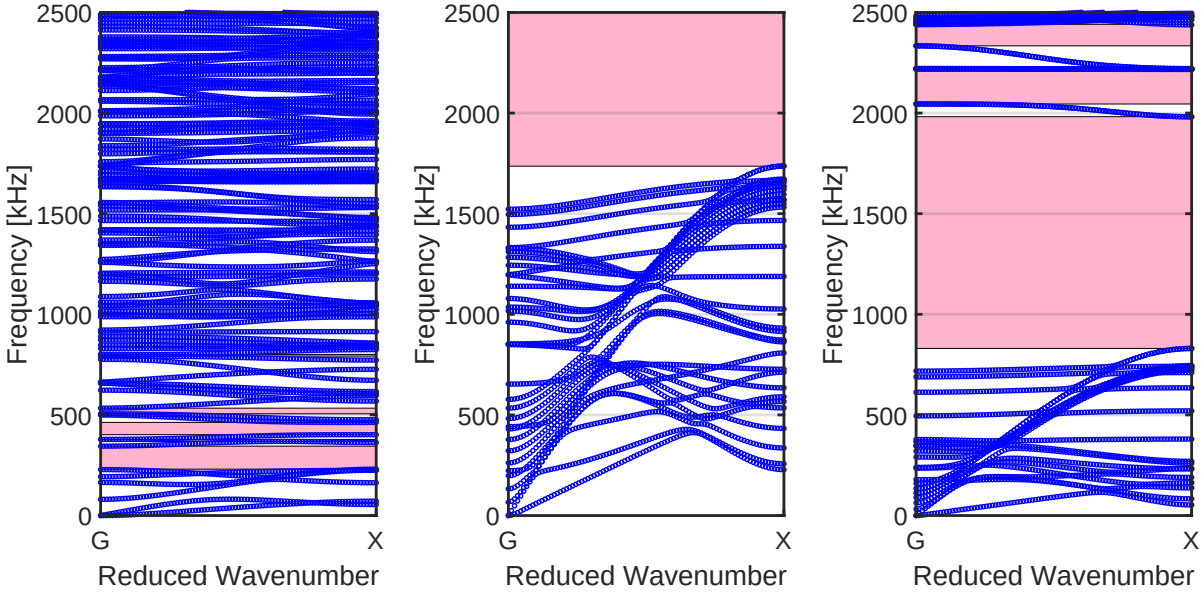


(a) (b) (c)

FIG. SM3: Numerically-predicted dispersion band structure for the (a) A1, (b) A2 and (c) A3 regions.

the waves with $f \geq f_1$ allowing on the other hand $f_0$ to pass through the barrier (BGs are highlighted by light pink rectangles).

### C. Propagation LtR and RtL

With the design described above we performed a Left to Right (LtR) and Right to Left (RtL) propagation simulation experiment. In Fig. SM5 the spectral analysis of the signals for LtR (a-d) and RtL (e-h) propagation are reported, respectively. With respect to Fig. 2 of the main text we added the FFT magnitude in the right cavity. As can be noted the diode functionality is confirmed by the fact that the component $f_1$ propagates from LtR, while no signal is detected at the receiver when the propagation is in the other direction.

## III. DISCUSSION ON THE EFFICIENCY OF THE DIODE

We performed an additional analysis on the efficiency of the presented device. The design, the choice of the intensity of the nonlinear source, the dimension of the three different zones

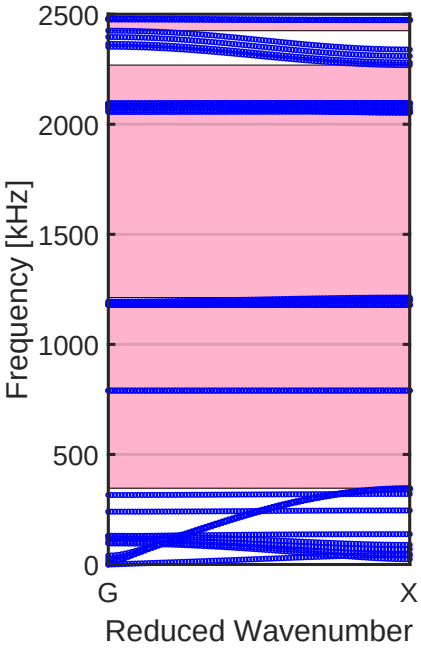


FIG. SM4: Dispersion diagram for the FB2.

of the device can change and significantly influence the results, due to the possibility to exploit resonances of the sample and to optimize the characteristics of the nonlinearity (position, form, excitation, etc.). Here, we demonstrate how the efficiency of the device can be tuned and evaluate its dependence on the main parameters.

Taking for simplicity a quadratic nonlinearity, as stated in the main text, the generation of the frequency mixing in the sidebands is proportional to the product of the amplitudes of the two mixed frequency sources ($A_1$ and $A_2$ for sources $S_1$ and $S_2$, respectively), through the nonlinear parameter ($\beta_1$). Then, we expect the amplitude of the sub-harmonic, $f_0$, to be

$$A_0 \propto \beta_1 A_1 A_2 \tag{SM1}$$

Similarly, for the generation of the harmonics of $f_0$ in the second nonlinear zone (with nonlinear parameter $\beta_2$), we expect the amplitude of the output to be

$$A_{out} \propto \beta_2 A_0^2 = \beta_2 \beta_1^2 A_1^2 A_2^2. \tag{SM2}$$

From Eq. SM2 it is evident that the efficiency, $e$, which can be defined as the ratio between the squared input and output amplitudes, can be approximately estimated as:

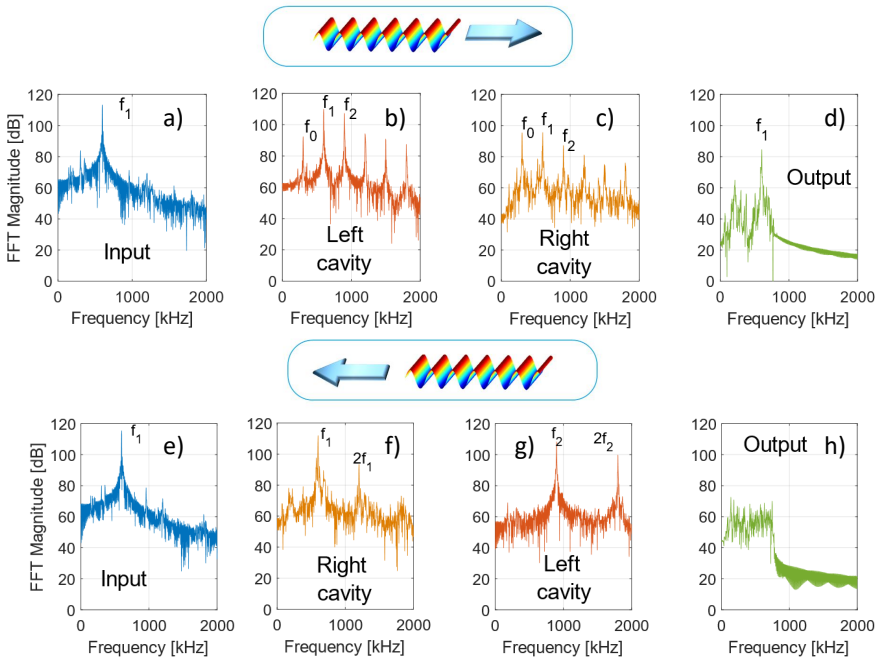


FIG. SM5: Spectral content of the wavefield during Left to Righ (a-d) and Right to Left (e-h) propagation.

$$e = \frac{A_{out}^2}{A_1^2} \propto \beta_2^2 \beta_1^4 A_1^2 A_2^4. \tag{SM3}$$

To verify this hypothesis, we performed a specific parametric study of a 1-D device working at $f_1 = 1.2\,\mathrm{MHz}$ (so that $f_2 = 1.8\,\mathrm{MHz}$ and $f_0 = 0.6\,\mathrm{MHz}$). The principal propagating medium (the matrix) is an alluminium bar ($\rho_1 = 2700\,\mathrm{kg/m^3}$, $E_1 = 70\,\mathrm{GPa}$), 180 mm in length. The phononic crystal is realized by alternating layers of alluminium and a second material with reduced modulus and density ($\rho_2 = 200\,\mathrm{kg/m^3}$, $E_2 = 7\,\mathrm{GPa}$, e.g. wood). The three filtering barriers are designed by varying the characteristics of the unit cell (size and filling factor) as reported in Table III. FB2, in this case, is realized as a sequence of two phononic crystals ($\mathrm{FB2}_A$ and $\mathrm{FB2}_B$), in order to maximize the width of the filter and to cut frequencies above $f_0$.

To verify Eq. SM2 and estimate the intensity of the nonlinear parameters and proportionality between the two nonlinear zones, in order to obtain the desirable efficiency in this 1-D model, we performed a series of simulations varying the quadratic nonlinear parameters of

TABLE III: Geometrical parameters for the unit cell of the 1-D model.

| Barrier | Cell size [mm] | Width of the inclusion [mm] | Passing frequency |
|---|---|---|---|
| FB1 | 0.9 | 0.8 | $f_p \leq f_1$ |
| $FB2_A$ | 1.4 | 1.2 | $f_p < f_1$ |
| $FB2_B$ | 0.9 | 0.8 | $f_p < f_2$ |
| FB3 | 2.7 | 2.4 | $f_0 < f_p \leq f_1$ |

the two nonlinear zones ($\beta_1$ and $\beta_2$). As shown in Fig. SM6, simulations highlight the linear and quadratic dependence of the output vs input amplitudes on the nonlinear parameters.

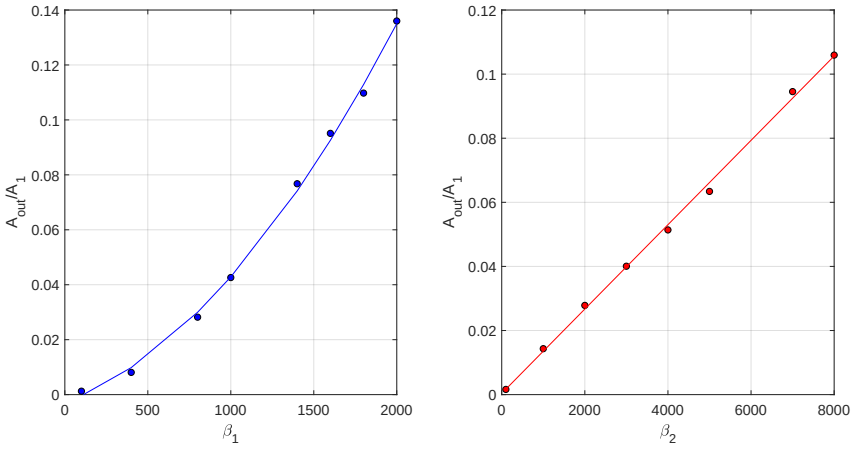


FIG. SM6: Numerical parametric study: (a) Dependence of Output/Input amplitudes as a function of nonlinear parameter $\beta_1$; (b) Dependence of Output/Input amplitudes as a function of nonlinear parameter $\beta_2$.

## IV. SAMPLES AND EXPERIMENTAL CONFIGURATION

A schematic representation of the experimental specimen is shown in Fig. SM7, along with its dimensions (in mm). The specimen consists of a 6 mm-thick aluminum plate with a 2D array of $4 \times 8$ cross-like cavities machined in its middle portion. The sample is obtained

via water-jet cutting starting from a unique pristine aluminum sheet, exhibiting linear elastic properties with the following nominal mechanical parameters $\rho = 2700\,\mathrm{kg/m^3}$, $E = 70\,\mathrm{GPa}$ $\nu = 0.33$.

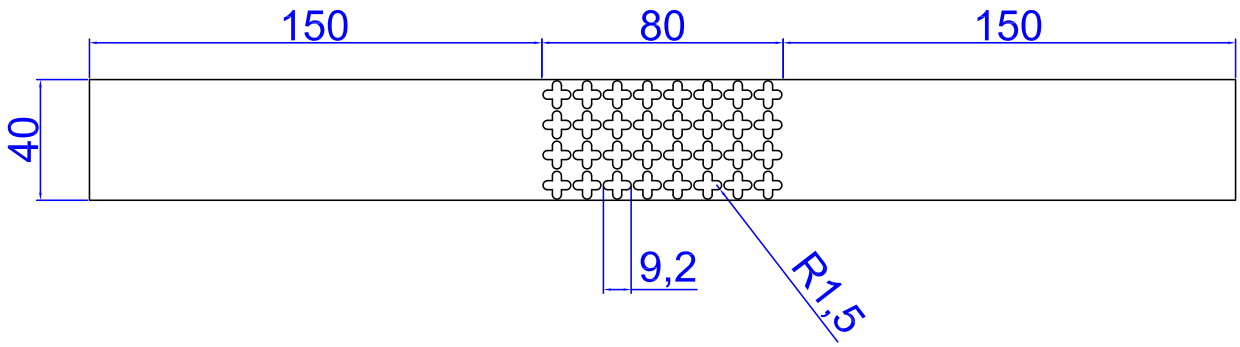


FIG. SM7: Schematic representation of the specimen composed of an aluminium plate with a phononic crystal region made of cross-like holes. Dimensions are in mm. Plate thickness is 6 mm.

The corresponding dispersion diagram of the periodic structure presented in Fig. SM7 is computed numerically applying the Bloch-Floquet periodic boundary conditions, which allow to consider only one unit cell [2]. A full 3D model is implemented to capture all the possible wave modes propagating in the structure. Cells are meshed by means of 4-node tetrahedral elements of maximum size $L_{FE} = 1$ mm in order to provide accurate eigensolutions up to the maximum frequency of interest.

The band structure is derived assuming periodic (in the $x$-direction) and free (in the $y$-direction) boundary conditions at the edges of the cell domain. Free boundary conditions are imposed at the top and bottom surfaces of the cell. The resulting eigenvalue problem $(\mathbf{K} - \omega^2\mathbf{M})\mathbf{u} = \mathbf{0}$ is solved by varying the wave vector $\vec{k} = \{k_x, k_y\}$ values along the first irreducible Brillouin zone boundary $\Gamma - X$ (since the periodicity is only in the $x$-direction).

Figure SM8 presents the band structures in terms of reduced wavevector $k^* = [k_x \cdot a/\pi$ with $a = 10$ mm (lattice geometrical parameters are given in mm in Fig. SM7). Two main BGs (light pink rectangles) exist in the $[0 - 250]$ kHz frequency range, with the lower one extending from 124 kHz to 175 kHz. The other extends from 191 kHz to 236 kHz, apart from very flat bands ranging from 201 kHz to 203 kHz. The experimental results are in excelent agreement with the numerical predictions (see Fig.SM8b).

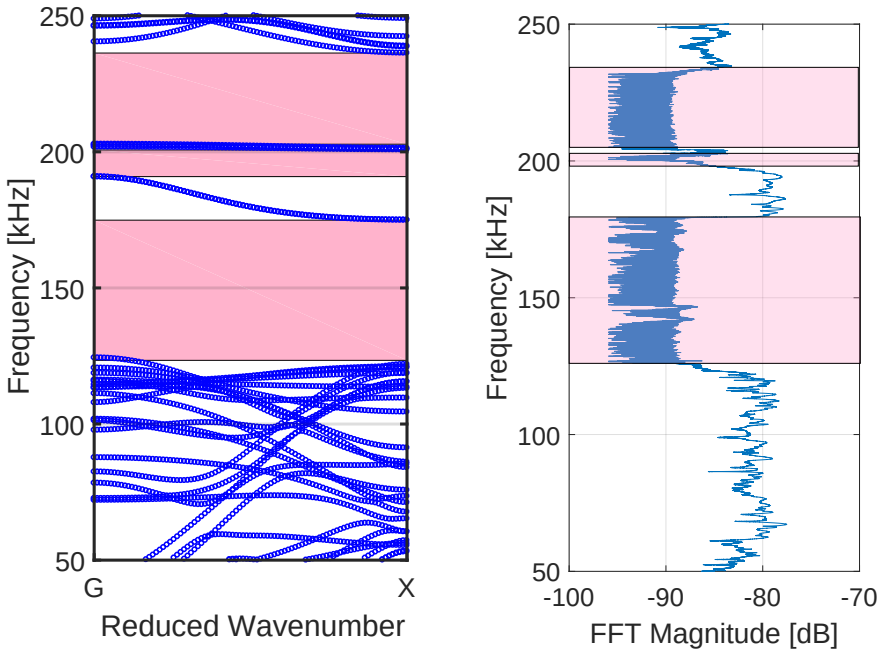


(a) (b)

FIG. SM8: Dispersion diagram for the unit cell used for the experimental investigation (a). FFT of the signal obtained with a propagation experiment.

## V. EXPERIMENTAL RESULTS

To verify the functionality of the experimental set-up, we study here the spectral content of the signal generated by the transducer $S1$ (Fig.SM9a), as it travels through the metastructure. Figs. SM9(b-d) show the FFT analysis of the wavefield recorded at three different points A1, A2 and A3 in the sample, as detected by the laser vibrometer: only the nonlinearity in the first cavity (NL1) is activated (no reciprocity breaking is expected in this case), so the only frequency that can travel from left to right is the frequency $f_0 = 75\,\text{kHz}$, generated by wave mixing in the left cavity. The small peak occurring at 450 kHz corresponds to the second harmonic of $f_2$, which is not filtered by the phononic crystal.

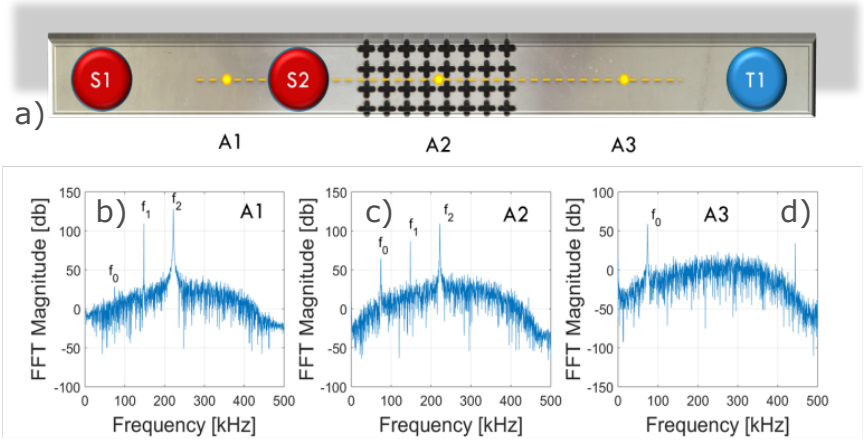


FIG. SM9: (a) Experimental device and setup. (b-d) Spectral content of the signal recorded at three different points A1, A2 and A3 in the sample, as detected by the laser vibrometer along the dashed line schematic (a).

---


[1] M. Miniaci, M. Mazzotti, M. Radzieński, N. Kherraz, P. Kudela, W. Ostachowicz, B. Morvan, F. Bosia, N. M. Pugno. Experimental Observation of a Large Low-Frequency Band Gap in a Polymer Waveguide, Front. Mater., **5**, 2018.

[2] M. Collet, M. Ouisse, M. Ruzzene, and M. Ichchou, Int. J. Solids Struct. 48, 2837 (2011).